Hydrol. Earth Syst. Sci. Discuss., 11, 3967–4015, 2014
www.hydrol-earth-syst-sci-discuss.net/11/3967/2014/
doi:10.5194/hessd-11-3967-2014

Hydrology and Earth System Sciences
Open Access
Discussions

Cloudiness and snow cover in Alpine areas from MODIS products

P. Da Ronco[1,2] **and C. De Michele**[2]

[1]Centro Euro-Mediterraneo sui Cambiamenti Climatici, Impacts on Soil and Coasts Division, Capua, CE, Italy
[2]Politecnico di Milano, Department of Civil and Environmental Engineering, Milano, Italy

Received: 5 March 2014 – Accepted: 7 April 2014 – Published: 10 April 2014

Correspondence to: P. Da Ronco (pierfrancesco.daronco@cmcc.it)

Published by Copernicus Publications on behalf of the European Geosciences Union.

Abstract

Snow cover maps provide an information of great practical interest for hydrologic purposes: when combined with point values of snow water equivalent (SWE), they allow to estimate the regional snow resource. Earth observation satellites are an interesting tool for evaluating large scale snow distribution and extension. In this context, MODIS (MODerate resolution Imaging Spectroradiometeron on board Terra and Aqua satellites) daily Snow Covered Area product has been widely tested and proved to be appropriate for hydrologic applications. However, within a daily map the presence of cloudiness can hide the ground, thus preventing snow detection.

Here, we considered MODIS binary products for daily snow mapping over Po river basin. Modeling the variability of snow cover duration, distribution and snow water equivalent is a first important step in investigating climate change impacts on the regime of the major Italian river. Ten years (2003–2012) of MOD10A1 and MYD10A1 snow maps have been analyzed and processed with the support of 500 m-resolution Digital Elevation Model (DEM). We firstly investigated the issue of cloudiness, highlighting its dependence on altitude and season. Snow maps seem to suffer the influence of overcast conditions mainly in mountain and during the melting season. Such a result is certainly related to satellite crossing times, since cloud coverage over mountains usually increases in the afternoon: however, in Aqua and Terra snow products it highly influences those areas where snow detection is regarded with more interest. In spring, the average percentages of area lying beneath clouds are in the order of 70 %, for altitudes over 1000 m a.s.l.

Then, on the basis of previous studies, we proposed a cloud removal procedure and its application to a wide area, characterized by high topographic and geomorphological heterogeneities such as northern Italy. While conceiving the new method, our first target was to preserve the daily temporal resolution of the product. Regional snow and land lines were estimated for detecting snow cover dependence on elevation. In cases when there were not enough information on the same day within the cloud-free areas,

HESSD

11, 3967–4015, 2014

we improved a temporal filter with the aim of reproducing the micro-cycles which characterize the transition altitudes, where snow does not stand continually over the entire winter.

In the validation stage, the proposed procedure has been compared against others, showing improvements in the performance for our case study. At the same time it results quite handy both in terms of input data required and computational effort.

1 Introduction

Climate change is expected to have a significant impact on water availability of snow-dominated regions (Beniston, 2003; Barnett et al., 2005). The discharges generated by mountain areas largely contribute to streamflows of many rivers that cross the most populated and economically developed regions in Europe. Several authors agree in predicting a shift of the hydrologic regime of the main European rivers, due to a changed behavior of the mountain valleys. Changes are predicted for Rhine (Shabalova et al., 2003; Lenderink et al., 2007; Hurkmans et al., 2010; Junghans et al., 2011), Rhone (Etchevers et al., 2002; Boé et al., 2009) and Danube (Hagemann et al., 2009). Focusing on Po river system, Alpine areas cover 35 % of the basin and contribute on average for 53 % of the total discharge (Vanham, 2012). Understanding the effects of atmospheric forcings on snow cover duration and distribution at the basin scale is a starting point for modeling climate change impacts on the hydrologic regime. Besides such variables can be considered reliable indicators of climate trends (Haeberli and Beniston, 1998; Beniston, 2003), since snow cover depths and distribution are not only the results of diurnal values of temperature and precipitation, but mostly a product of the history of these two variables from the beginning of the accumulation season (Beniston, 1997).

In this perspective, remote sensing can be useful for reconstructing recent snow variabilities in wide regions such as northern Italy. The use of snow cover maps for hydrological purposes is an effective tool, since the combination of a large-scale information

HESSD
11, 3967–4015, 2014

with local estimations or measurements of snow features allows to estimate the snow water equivalent (SWE) stored within a river basin (Molotch and Margulis, 2008; Bavera and De Michele, 2009). Moderate Resolution Imaging Spectroradiometers (MODIS) employed by Terra and Aqua satellites provide a Snow Covered Area product (SCA) with 500 m and daily resolutions, which consists in binary maps where snow is detected at the pixel scale. The accuracy of MODIS Snow Cover Products depends on region, season, snow condition and land cover type (Klein and Barnett, 2003; Maurer et al., 2003; Simic et al., 2004; Zhou et al., 2005; Tekeli et al., 2005; Ault et al., 2006; Parajka et al., 2006; Hall and Riggs, 2007; Liang et al., 2008). In Europe, Parajka et al. (2006) compared daily MODIS snow maps with in situ data of 754 climate stations over the whole Austria, reporting an average classification accuracy of 95 % on cloud-free days. The wide and heterogeneous Austrian territory presents similarities with our case study.

However, the primary limitation in using MODIS snow products is that no information on ground conditions is available in areas hidden by cloudiness. During a year clouds may obscure most of the study area, restricting the potentiality of using snow cover images. For example Parajka et al. (2006) indicated that, on average, clouds obscured 63 % of Austria in daily snow maps from February 2000 to December 2005. The advantage to benefit of a reliable product with daily temporal resolution is therefore conditioned to the ability of estimating the presence of snow in overcast conditions. With this target several procedures have been developed and tested in different regions (Parajka and Blöschl, 2008; Gafurov and Bárdossy, 2009; Parajka et al., 2010; Paudel and Andersen, 2011). On the basis of such results, we developed a cloud removal procedure which shows better performances respect to the existing approaches, and we tested it over Po river basin.

HESSD
11, 3967–4015, 2014

2 Case study: Po river basin

Po is the major Italian river and one of the most important fluvial system in Europe from an economic point of view. It flows more than 650 km eastward across northern Italy, from a spring seeping at Pian del Re, Piemonte, through a wide delta into the Adriatic sea between Venice and Ravenna. Its drainage area covers approximately 74000 square kilometers, of which about 71 000 located in Italian territory, a quarter of the national territory. The remaining area is located for the most part in Switzerland (Toce river basin) and for a smaller part in France. Considering the level of utilization of water resources for agricultural and industrial purposes, the Po basin is a focal point of the Italian national economy.

Through its tributaries, the river drains mountain regions that reach altitudes above 4700 m a.s.l. in the Aosta valley (Fig. 1a). The hypsographic curve for Po river basin is given in Fig. 1b, where the *x* axis represents the surface areas (or relative surface area) which lies above and below a marked elevation while the *y* axis represents the elevations above the sea level. Such curve has been obtained from a DEM with 500 m spatial resolution. Figure 1b shows that more than 30 % of the area lies above 1000 m a.s.l., where snow dynamics are expected to have an important effect on the hydrologic cycle. The spatial and temporal evolution of the snow cover over the basin is thus one of the core issue for characterizing the hydrologic regime of the river, as well as for assessing its susceptibility to changing climate conditions.

2.1 MODIS snow-covered area products

The Spectroradiometers employed by Terra and Aqua satellites provide a snow covered area product (SCA) available in the National Snow and Ice Data Center (NSIDC) Distributed Active Archive Center. Maps belong to Collection 5 (Riggs et al., 2006) of MODIS snow products, released after the reprocessing which began in September 2006, showing improvements in the cloud mask product and improved screening for erroneous snow. Cloud masks are derived from MOD35, with daily temporal and 1 km

HESSD
11, 3967–4015, 2014

spatial resolution. Each pixel not masked by clouds is processed by the snow-mapping algorithm (Hall et al., 2001). It consists of some tests and decision rules that identify snow in each pixel of a MODIS image, and it is able to detect snow even in dense forests (Klein et al., 1998). The procedure for snow detection employed by MODIS Snow Products works on a pixel-by-pixel basis involving a grouped-criteria technique which uses the Normalized Difference Snow Index (NDSI) and other spectral threshold tests (Hall et al., 1995; Klein et al., 1998; Hall et al., 2001). MOD10A1 is a set of daily MODIS snow products available from February 2000 that contains daily snow maps from the Terra satellite, while MYD10A1 are similar products derived from MODIS on board the Aqua satellite, launched in May 2002. MOD10A1 and MYD10A1 provide daily snow albedo (Klein and Stroeve, 2002), fractional snow cover (FSC) (Salomonson and Appel, 2004, 2006) and the snow cover daily tile (SCA). The last product contains a binary information (snow/not snow) for each pixel. Our choice of adopting the binary product instead of the fractional one is due to its wider use in the last decade, that produced several assessments of its reliability (Hall and Riggs, 2007). MOD10A1 and MYD10A1 are generated through a mapping of pixels derived from the swath products MOD10L2 and MYD10L2 to their geographic locations in a MODIS-specific global sinusoidal projection.

2.2 Data pre-processing

Daily snow products MOD10A1 and MYD10A1 are downloaded from NASA's EOSDIS "Reverb". Snow cover daily tiles are provided in sinusoidal projection. Tiles are 10° by 10° at the equator. The study area is entirely covered by the h18v04 tile. Snow maps of Northern Italy are then projected into UTM WGS84 coordinate system, Zone 32 band T, and overlapped with a mask of Po river basin. We reclassified MODIS snow cover maps from original pixel classes (Riggs et al., 2006) to four classes: snow, land, cloud and others. "Missing data" and "No decision" fields are treated equally to cloud pixels, where snow presence has to be investigated.

HESSD
11, 3967–4015, 2014

We preprocessed daily Terra and Aqua SCA maps from January 2003 to December 2012. Clear-sky days provide an indicative value of the fluctuation of the snow covered area throughout the year. For instance on 1 January 2005 snow is about 30 % of the clear-sky pixels, while this percentage decreases to 5 % at the beginning of May (average elevation of the snow-covered pixels of 2640 m a.s.l.) and less than 0.5 % at the end of June, when the mean altitude of the snow covered cells exceeds 3260 m a.s.l. Analyzing the most cloud-free days without snowfalls in the lowlands of the 2004/2005 and 2005/2006 winter months, values between 20 and 30 % seem a representative range for the long-lasting snow covered fraction of the basin. Notice that the hypsographic curve of Po Valley had shown that about 30 % of the area lies above 1000 m a.s.l. and 20 % above 1500 m a.s.l. Figure 2a shows a comparison between snow observed by the Aqua MODIS on 28 June 2005 and a digital map of Lombardy's glaciers. The latter is the result of processing and comparison of areal data taken from orthophotos (1999–2007), and from glaciological registers. Given that at the end of June snow cover extension has not yet achieved its annual minimum size, it is seen how the cores of the glaciers are contained in boundaries identified as snow by MODIS. A similar view is proposed in Fig. 2b. Here, we generated polygon-shaped glaciers from Aqua and Terra snow maps of 18 July 2012. Such areas are then overlapped to orthophotos taken about a month later. The proper identification of glacier boundaries can be interesting even for validation purposes.

3 Cloud removal procedure

Aqua/Terra snow maps present a cloud coverage, ranging from 0 to 100 % of the domain depending on the day. Several procedures have been proposed for mapping snow beneath clouds. Such methods are based on spatio-temporal combination of data and would ensure the availability of maps with daily temporal resolution. Contrary to the case studies in Gafurov and Bárdossy (2009) (Kokcha basin: elevations range from 416 m a.s.l. up to 6383 m a.s.l., about 75 % of the basin area lies above

HESSD
11, 3967–4015, 2014

above 2000 m a.s.l.) and Paudel and Andersen (2011) (Trans Himalayan region: 96 % of the area lies in the elevation zone above 3000 m a.s.l., with 43 % of the area above 5000 m a.s.l.), many European rivers drain basins which cover altitudes from the lowlands up to 4000 m a.s.l. in the Alpine region. The majority of the drainage areas corresponds to elevations where snow dynamics are fast and several snow accumulation – snowmelt cycles may happen over the year. Some of the assumptions made by Gafurov and Bárdossy (2009) and Paudel and Andersen (2011) do not fit suitably to our case study. A spatio-temporal combination of MODIS image for cloud reduction was tested by Parajka and Blöschl (2008) over the whole Austria, a territory more similar to our case. Testing some backward filters, they obtained a minimum accordance with ground observation of about 92 % in relation to a seven days temporal filter. The latter was applied after merging Aqua and Terra images. However, temporal filters leave a percentage of cloudiness depending on the allowed temporal window from which the procedure can derive information to add to the assessment day. Moreover, the accuracy of this method is highly dependent on the period of the year (Parajka and Blöschl, 2008). During the winter, snow processes in mountains are slower and in the middle of the summer snow maps tend to a steady layout with snow over glaciers and snowfields. On the contrary, both in spring and autumn ground conditions change faster, due to snowfall or snowmelt which determines several land/snow micro-cycles on the transition altitudes. Later procedures tried to improve the performances of a mere temporal filter in other regions (Gafurov and Bárdossy, 2009; Parajka et al., 2010; Gao et al., 2010). Some of them allow even to clean up the whole domain from clouds.

We integrate and improve steps proposed by different authors in order to maximize the performance of the procedure when applied to Po basin. This region presents peculiarities which require the adjustment of a procedure to this specific environment. At the same time we avert the requirement of data from other satellites or information on land cover types: this solution involves only Aqua and Terra daily maps and a DEM of the domain.

HESSD
11, 3967–4015, 2014

3.1 Step 1

The first step crosses Terra with Aqua information of the same day. The source map is the daily binary product in MOD10A1 provided by MODIS on board the Terra satellite. Aqua MYD10A1 images are involved in order to classify pixels obscured by clouds in the source Terra images. The choice of a source map is important since Terra and Aqua products may present inconsistencies due to the different crossing time of these satellites. Aqua observes the considered area few hours later, in the afternoon, when cloudiness usually increases and ground condition might be changed. Once chosen MOD10A1 as source, MYD10A1 intervenes only by adding information for pixels not already identified as snow or land by Terra MODIS, while Terra maps rule any incongruity. The choice of MOD10A1 as the main product descends from several validations it has been subjected (Hall and Riggs, 2007).

We name $\mathrm{Map_T}(d, x, y, z) = S$, L or C respectively a snow, land or cloud cell in the Terra snow product, centered in (x, y, z) at the day d. Similarly we name $\mathrm{Map_A}(d, x, y, z) = S$, L or C a snow, land or cloud pixel within Aqua map. The first step returns $\mathrm{Map_1}(d)$ composed of snow, land, and cloud pixels ready to be processed by the next. Since we are looking for a daily map and this passage overlaps maps of the same day, it actually does not introduce any loss of accuracy if we suppose that both products have a similar quality.

3.2 Step 2

The second step estimates ground cover deriving information from the neighboring days but only when such conditions can be considered stationary over an appropriate temporal window (Gafurov and Bárdossy, 2009). For each cloud cell $\mathrm{Map_1}(d, x, y, z) = C$ the algorithm analyzes its classification in the snow maps of the previous two days and of the next two days. If $\mathrm{Map_1}(d-1)$, $\mathrm{Map_1}(d-2)$, $\mathrm{Map_1}(d+1)$, $\mathrm{Map_1}(d+2)$ contain new information for that cell and agreement is found between the classifications within a maximum time interval of three days, such observed cover is

HESSD
11, 3967–4015, 2014

used for classifying the pixel of $\mathrm{Map}_1(d)$. This implies that if a cell at $d-1$ is marked as snow covered, $\mathrm{Map}_1(d-1,x,y,z)=S$, and snow is observed also one or two days after d, the cloud pixel C is converted into snow by step 2. The same correction intervenes if correspondence is found between $d-2$ and $d+1$. The same applies for land observations. The step is not involved whenever inconsistency between ground conditions does not allow to draw likely conclusions on d: for example, if the sequence of observations is $\mathrm{Map}_1(d-1,x,y,z)=S$, $\mathrm{Map}_1(d,x,y,z)=C$ and $\mathrm{Map}_1(d+1,x,y,z)=L$ the algorithm does not apply any correction to the cell, letting the subsequent steps the chance of determining whether there is snow. The basic assumption which justifies this filter is based on the concept that if both the previous and the next days have the same surface cover, such condition is kept in cloudy weather (Gafurov and Bárdossy, 2009). Even if snowmelt may occur during overcast days, direct shortwave radiation is shielded by clouds that reduce the solar energy available for the melting process. On the other side, when an area is snow free during the previous and the next remote observations, it might be snow covered in the meantime, but snow amount and duration would not be determinant for hydrological purposes.

3.3 Step 3

The third step is based on elevation dependence of snow cover. The concept is to find the right altitude below which we can assume the cloud mask to hide land pixels, and the elevation above which all pixels are likely snow. On the one hand, temperature is usually linked to altitude by a linear relationship depending on temperature lapse rate. Snow distribution in mountain is the result of snowpack conditions evolving during the whole winter season; particular situations such as temperature-inversion may occur, but they are not expected to produce a determinant impact on snow patterns. On the other hand, temperature is frequently used to determine both the aggregation state of precipitation and the melt rates (Schaefli et al., 2005). The widely used temperature-index melt model (Hock, 2003; Ohmura, 2001) is based on the assumption that melt

HESSD
11, 3967–4015, 2014

fluxes are linearly related to air temperature, which is seen as an integrated index of the total energy available for melting.

Step 3 involves a criterion similar to the regional snow line and land line approach proposed by Parajka et al. (2010). The regional snow line, μ_s, is the mean altitude of snow covered pixels within the basin. The regional land line, μ_l, is defined similarly as the average altitude of land pixels, calculated over the cloud-free part of the domain. However, our step 3 adopts even a subdivision of the area per aspect classes. Depending on its exposure, each cell is matched with one of the four classes N, S, W, E. Thus, we allow classes to have their own snow and land line altitudes, elevations that may be affected by solar radiation amount. This measure can help in reproducing accurate snow profiles during the melting seasons, when snowfalls are rare and direct shortwave radiation rules the melting process (Hock, 1999). Shortwave radiation may be adopted as the main representative of global radiation, since the other components depend on it, directly or indirectly (Dubayah and Rich, 1995; Kumar et al., 1997). Once individuated μ_s and μ_l, step 3 turns into snow the cloud mask standing above the snow line and into land the part below the land line:

$$\mathrm{Map}_2(z \geq \mu_s) = C \longrightarrow \mathrm{Map}_3(z \geq \mu_s) = S \quad (1)$$

$$\mathrm{Map}_2(z < \mu_l) = C \longrightarrow \mathrm{Map}_3(z < \mu_l) = L \quad (2)$$

$$\mathrm{Map}_2(\mu_l \leq z < \mu_s) = C \longrightarrow \mathrm{Map}_3(\mu_l \leq z < \mu_s) = C. \quad (3)$$

We avoided a discretization of the domain in sub-basins or homogeneous landscape units (Paudel and Andersen, 2011), to make the procedure independent from additional data. Other proposals define such threshold altitudes focusing on the highest land pixel and the lowest snow pixel (Gafurov and Bárdossy, 2009; Paudel and Andersen, 2011). Here, the limitation results from the exportation of a local assessment, linked to a single cell wherever located, as information on snow distribution over the whole study area. Within a densely urbanized basin, isolate snow-free areas may stand at very high altitude also in winter, thus shifting upwards the assessment of the snow line. Besides any error of MODIS Snowmap algorithms, which would classify isolate land

HESSD
11, 3967–4015, 2014

cells where snow is expected (e.g. a snow area lying in shadow not individuated by the snow mapping procedure) or vice versa (e.g. the misclassification of cirrus clouds as snow in the period between May and October), may prevent the effectiveness of step 3.

We introduced some limitations to the intervention of the regional line method. First, we allowed its application only in cases when the basin is at least 50 % cloud-free, in order to ensure a representative estimation of the actual snow and land average altitudes. Furthermore the snow line is calculated only if observed snow pixels are at least 5 % of the observed land pixels. 5 % is a representative percentage of the snow pixels found in maps during the late spring on some cloud-free days. Throughout the winter, the ratio between the number of pixels classified as snow and the number of snow-free pixels should be higher even in presence of clouds. If this condition is not met few snow areas are observed and their mean altitude can not be considered representative of the actual snow pattern for the whole study area, even when the sky is enough clear. With the same purpose we let the algorithm skip the assessment of the snow line in summer (from June to September), when the percentage of snow areas is very low. The latter measure is designed to avoid errors arising from the classification of some clouds as snow; this misclassification may become determinant in assessing the snow line, because of the lower number of actually snow-covered cells.

3.4 Step 4

Further passages must solve the transition band which lies between land and snow regional lines, and all the other cases when step 3 is not involved. Until this point the target of maintaining snow maps with daily temporal resolution is kept. Step 1 and 3 bring down cloudiness using information from the same daily map, while step 2 uses data from close days but only when ground condition can be assumed constant over time.

Step 4 uses information derived from selected time window. Ground conditions are thus approximated as stationary over a chosen period. The more we expand this temporal window, higher is the probability that ground conditions are changed within

HESSD
11, 3967–4015, 2014

(Parajka and Blöschl, 2008). We introduce a six day backward temporal filter on step 4. A cloud pixel is classified to snow or land depending on the last time it was observed within the previous period. The threshold of 6 days ensures a temporal resolution of the map higher than MODIS 8-day snow products, which contains the maximum snow cover extent over an 8-day window. Looking at the results provided by a 5-day and a 7-day filter for Austria (Parajka and Blöschl, 2008), six day could be a good compromise to ensure a good level of accuracy while bring down cloudiness to a very low percentage.

3.5 Step 5

The remaining clouds are processed by a fifth step, named "macro-cycle", similar to the last step of Gafurov and Bárdossy (2009). It works at the pixel scale, by investigating the snow annual cycle for each cell. Several features of the location (eg the exposure to solar radiation and the land use) intervene in the snowmelt process; for these reasons, a pattern designed specifically for each cell can be an advantage in detecting the individual behaviors. The first target is the right identification of an accumulation season and a land-season per pixel. As accumulation season we define a time period when a pixel is expected to be snow covered. Even if land observations are possible meanwhile, it is assumed that over the accumulation months the pixel is likely covered by snow when still masked by cloud after step 4. On the other side, once individuated the "land season", every cloud observation not processed by the previous steps will be changed to land. The snow-start and land-start flags are individuated basing on an improved approach described hereafter. We used output maps by step 1, since we prefer that these two time frames come from snow actually observed from a satellite. Given a pixel, the accumulation-start flag is individuated as the first day when snow is observed, providing that it is followed over time by other n_s snow observations not interrupted by land. This means that the accumulation season starts at the first snowfall, but only if the pixel is still snow covered or hidden by clouds on next days, until the n_s^{th} + 1 snow observation is met. The aim is that of avoiding false identifications

HESSD
11, 3967–4015, 2014

of the accumulation-start flag due to occasional snowfalls that may occur, even at low altitudes. The threshold number of snow days n_s is set depending on elevation, using three elevation bands, with a mean value of $n_s = 2$ for the transition elevations. Such threshold decreases with altitude, since at lower elevations it is likely that the first snow detection is due to a an occasional event, while in the higher areas one or two snow observations uninterrupted by land seem an appropriate signal of the beginning of the winter. The same rule is adopted for individuating the land-season start flags, in spring or summer (Fig. 3). Here, the threshold value n_l is set increasing with elevation, to prevent situations in which exceptional land detections in the uplands due to anomalous high temperatures are taken as indicators of the absolute end of the snow period. Moreover, the choice to involve more days after the first land/snow observation protects from possible misclassification from MODIS algorithms, which may confuse some types of cloud with snow also where and when snow is not expected. We specify that a snow accumulation period is defined only for those areas lying at altitude higher than z_T = 600 m a.s.l.: the threshold altitude has been chosen considered some studies on snow duration in the Alps (Beniston, 1997; Valt and Cianfarra, 2010). As consequence, pixels not already classified and located lower than z_T are converted to land regardless of the period year. At low elevations long-lasting snow covers are infrequent, while several short cycles of accumulation-melt may occur. In these situations snow depths remain relatively thin, thus our choice may lead to a slight underestimation of the snow amount which would not justify the delineation of each brief snow cycle.

At high elevations, snow cover develops according to a year cycle composed of two macro-periods, evolving from the accumulation to the melt season. However, the life of snow cover is highly affected by altitude, which provides an indication of the persistence of low temperatures. Italian Alps are mostly distributed on transition altitudes, where several land/snow micro-cycles happen, characterized by snow durations from few days to several months. The separation of the year into two seasons per pixel may lead to rough errors of snow overestimation at the beginning of the winter season and

HESSD
11, 3967–4015, 2014

underestimation after first (but maybe not last) melting completes. That is why step 5 is preceded by a temporal filter in step 4.

4 Results

Here, we firstly provide some considerations about cloudiness and its negative effects on snow mapping in Alpine areas. Then, we show the results of the cloud removal methodology applied to the case study. Finally, the performance of the procedure is assessed in term of efficacy and accuracy.

4.1 Cloudiness over Po basin

We studied the issue of cloudiness to better understand how much it would restrict the fruition of remote sensing products with daily temporal resolution. Once reclassified each snow map in three classes (cloud C, snow S, land L), let $N_{c,d}(Z > z_T)$, $N_{s,d}(Z > z_T)$, $N_{l,d}(Z > z_T)$ be the numbers of cloud, snow and land pixels included in the map of day d, for elevations greater than z_T. $N_{tot}(Z > z_T)$ is the sum of $N_{c,d}(Z > z_T)$, $N_{s,d}(Z > z_T)$ and $N_{l,d}(Z > z_T)$. We get that

$$C_d(Z > z_T) = \frac{N_{c,d}(Z > z_T)}{N_{tot}(Z > z_T)} \quad (4)$$

represents the percentage of area hidden by clouds within the basin, observed on the day d. The variable C_d ranges from 0 to 1 over the year, depending on the weather. The histogram of its absolute frequency (0–365/366 days) is plotted in Fig. 4, for 2004. The distribution descends from the relationship between the spatial scale of atmospheric disturbances and the size of the basin. As it can be seen, the most frequent values are those wherein the domain is covered by cloud for more than 90 % or for less than 20 %. The mode of the distribution can be estimated around 95 %. The peak is even more evident analyzing Aqua images. The same happens for all the other years: it follows that

HESSD
11, 3967–4015, 2014

in cloudy whether usually the Po Valley lies entirely beneath clouds, without information for snow mapping from MODIS.

The mean annual value C_a is obtained as

$$C_a(Z > z_T) = \langle C_d(Z > z_T) \rangle = \frac{\sum_{d=1}^{n_d} C_d(Z > z_T)}{n_d} \quad (5)$$

where n_d is the number of recorded days for that year. For $z_T = 0$ m a.s.l. the basin is considered in its entirety. Processing MOD10A1 and MYD10A1 products of ten years (2003–2012) we got that the mean annual cloud-covered part of the basin corresponds to a percentage between 44 and 56 % for the Terra MODIS and between 46 and 59 % for the Aqua MODIS. These values are slightly lower than those found by Parajka et al. (2006) for Austria. The higher percentages found in the Aqua images depend on the fact that Aqua crosses northern Italy few hours later than Terra, in the afternoon, when cloudiness usually increases. In both cases these rates exceed 60 % analyzing only the Alpine regions located at elevations higher than 1000 or 2000 m a.s.l. (Table 1); such result is certainly related to the time of the day when these satellites cross the region (between the late morning and the afternoon). This confirms the evidence that in afternoon clouds usually insist especially over mountain areas. The effect is probably related to cumulonimbuses, forming from water vapor carried by upward air currents, whose rising is hampered by orography. At the same time air circulation in the valleys may contribute in cleaning low altitudes from clouds. The influence of topography is particularly evident in Fig. 5: here, we plotted the number of cloudy days per pixel recorded by Terra MODIS. It is possible to notice how cloud pixels show pattens related with elevations (see Fig. 1a for the DEM). Similar patterns occur even in the other years, but they are not reported here for brevity.

From Table 1 the values of average annual cloudiness over different thresholds confirm that the probability of being masked by clouds increases with altitude. Since uplands are also those where snow is expected in winter and spring, the problem of

HESSD
11, 3967–4015, 2014

cloudiness has a significant (and adverse) impact on the number of days in which the presence of snow can be detected.

Average values of cloudiness can be calculated per quarter (or per month), in order to point out whether a seasonal trend exists (Tables 2, 3). While considering the entire domain JAS (January-August-September) is characterized by largely lower values of cloudiness, the same trend does not apply for the part which lies above 1500 m a.s.l.. On the contrary, the mountain zone presents similar cloud cover percentages in the first, third and fourth quarters, but higher values are found in all springs.

Overall, these results highlight how clouds appear very intrusive for the daily products. Chosen a random pixel within the basin, we can conclude that it generally spends more than half of the days obscured by clouds. This implies that a cloud removal procedure will lead to estimate ground condition on about half of the days. Moreover, considering only mountains, cloudiness in spring reaches a seasonal average in the order of 70 %. The behavior of Alpine valleys in term of snow duration and distribution will be more complicated to detect specially during the melting season, when methods for cloud filtering will play a key role. Unfortunately, spring is even the period when snow patterns are more interesting from an hydrologic point of view.

4.2 Performance of the cloud removal procedure

The performance of the procedure is assessed here. Firstly, it is investigated the efficacy of each step, which is its contribution in terms of image cleaning from clouds. Then, we focus on accuracy of the steps and of their application in series.

4.2.1 Efficiency

Ten years of MODIS data have been processed. Table 4 summarizes the mean annual percentage of cloud cover C_a remaining after each step, proceeding from the source Aqua and Terra products to the final, removed-cloud, map.

HESSD
11, 3967–4015, 2014

The first step combines two "observed" daily maps (Aqua and Terra snow cover tiles): hence column "Step 1" represents the average annual fractions over which snow presence has been estimated using information from close days or cloud-free areas. This value is usually lower than 0.4, thanks to the well known efficacy of combining Aqua and Terra data (Parajka and Blöschl, 2008; Gafurov and Bárdossy, 2009). Step 2 is still based on recorded images, but maps are those of neighboring days. This step, introduced by Gafurov and Bárdossy (2009), proves to be very effective, since after its intervention the remaining mean cloudiness generally decreases to less than 30 %. Step 3 involves the regional snow and land lines, and results in an average decrease of the cloud mask between 3 to 5 %. This could seem a weak contribution; however, it should be considered that step 3 is involved only in days when clouds hide less than 50 % of the basin. Such condition is met on slightly more than half days per year; as consequence, its contribution on these dates is largely higher than it may seem looking at the average annual values. Moreover, the snow line is not used from June to September. On monthly average, it is clear that the intervention of step 3 is not negligible in winter (Fig. 6).

The regional snow and land lines are shown in Fig. 7 for 2003 (Fig. 7a) and 2008 (Fig. 7b), during the period January–May. Here, there are reported also the daily altitudes of the highest land pixel and of the lowest snow pixel in order to appreciate the difference with a second approach for delineating snow and land lines (Gafurov and Bárdossy, 2009; Paudel and Andersen, 2011). It appears that the effectiveness of this step highly increases while assessing such altitudes through average elevations: mean regional elevations of snow are everyday lower than the altitude above which all pixels are snow. The same applies for land areas, whose average elevation is ordinarily higher than the lowest snow. In Fig. 7, the rising of snow average altitude is related to melting, while lowerings are caused by snowfalls over low elevations that bring down the mean values. Figure 7a allows to point out the faster variability of the snow line in spring, when snow processes are faster but occasional snowfalls even occur. On the other side, the fluctuations of the maximum land elevation are always wider, especially

HESSD
11, 3967–4015, 2014

in winter: this is due to the fact that such estimate can be highly influenced by anomalous local conditions, or misclassification errors from the source MODIS product. The trend of the minimum snow elevation shows that throughout most of the winter Aqua and Terra maps contain at least one snow cell around the see level. This could be a result of specific local conditions occurring somewhere within the wide domain, as well as classification errors by MODIS Snowmap (Hall et al., 2001).

While the first 3 steps proceed in series (i.e. the output map of each is the input of the following), step 4 uses the most recent observation for each pixel (produced by step 1), as long as it falls within the previous week. Such operator is the busiest and reduces the mean annual values of cloud coverage to 2–4 %. Step 5 completes the cloud removal. Considered the average annual cloudiness filtered by the last step (2–4 %), it seems to entail a little effect; conversely its involvement is crucial, since it takes care of all those situations when cloudiness insists over the same area for several continuous days. On some dates the percentage of clouds remaining after step 4 are even higher than 10 %.

To highlight whether there are monthly differences in the effectiveness of each step, Table 5 contains average cloud cover fractions C_m per month remaining step by step. The values refer to 2010. Figure 6 shows the same results plotted for 2007 (a) and 2009 (b). The vertical distance between points of different steps represents the average values of cloudiness removed by the middle passages (eg the distance between a point on line "step 3" and a point on line "step 2" is the mean monthly contribution of step 3; the distance between a point on line "step 1" and a point on line "step 4" is the mean monthly contribution of steps 2 and 3). Line "step 4" is the mean percentage of cloudiness treated by step 5. Heavy seasonal patterns are difficult to note; nevertheless two remarks seem appropriate. First, we note an expansion of the band between line "step 3" and line "step 2" during the winter. Such contribution represents the intervention of step 3; the enlargement stems from the fact that the regional snow line in winter is located al lower elevations and so enhances the number of cloud pixels lying over (then classified as snow). On the contrary, the annual fluctuation of the regional land line is moderate, ruled by the wide plain area which experiments only occasional

HESSD
11, 3967–4015, 2014

snow covers (Fig. 7). Accordingly, the transition elevations between the regional lines, where step 3 does not act, restricts in winter.

A second consideration refers to the behavior of step 5 (distance between line "step 4" and the *x* axis): its average monthly contribution can exceed the 10 % in periods characterized by very high cloud cover rates. The explanation lies in the fact that high monthly percentages normally entail several continuous days of widespread cloudiness, which reduce the probability of finding data in the previous week. A similar situation appeared for Austria in Parajka and Blöschl (2008), using 5 and 7 day temporal filters in the period 2003–2005. Thank to this result, the importance of a step able to close the procedure is more clear.

Figure 8 shows the result of the procedure run on 27 March 2003. Here, step 4 basically closes the procedure, thus the final product by step 5 is not shown. It is possible to appreciate changes in cloud distribution on the crossing times of Aqua and Terra: in this case Aqua map does not provide additional data. Step 3 contributes in cleaning the very high and very low elevations, thanks to the regional lines, without affecting the transition band. The removed-cloud map by step 4 sheds light on snow distribution and its dependence on topography at the beginning of the spring.

4.2.2 Accuracy

We check the accuracy of the procedure following the methodology proposed by Gafurov and Bárdossy (2009), and used even in Paudel and Andersen (2011). Some cloud-free days, henceforth considered as "truths", are selected and covered of wide cloud masks. Such cloudiness is borrowed from dates when both Terra and Aqua products experiment overcast conditions. Then, the procedure is applied to the maps, in order to reclassify the additional clouds. Finally, the removed-cloud product is compared with the clear-sky Terra map. In this stage we are not interested in the reliability of the source MODIS products, which is a widely studied issue (Hall and Riggs, 2007). This way of checking the accuracy seems thus appropriate since it does not introduce misclassification errors coming from Snowmap algorithms, as it may happen when

HESSD
11, 3967–4015, 2014

comparing the output against ground data from weather stations (Parajka and Blöschl, 2008). The use of observed layouts of cloudiness ensures that Aqua and Terra maps assigned to the procedure correspond to configurations that may occur. Once chosen the cloudy day, Aqua clouds are overlapped to the clear-sky maps from Aqua. The same is done for Terra maps.

Given a clear-sky image at day d, fictitious cloudiness introduces an additional number of cloud pixels, ΔN_c, within the domain, whose percentage is

$$A_d = \frac{\Delta N_c}{N_{tot}}. \quad (6)$$

ΔN_c is calculated as the number of cloud pixels in the masked image that were cloud free in the source map. With $A_{d,A}$ and $A_{d,T}$ we will refer respectively to the additional cloudiness on Aqua and Terra images. N_{tot} represents the total number of cells included in the basin. Thus the percentage of cloudiness in the masked Terra map is

$$C_{d,T} = \frac{N_{c,T} + \Delta N_{c,T}}{N_{tot}} \quad (7)$$

where $N_{c,T}$ is the number of cloud pixels in the clear-sky Terra product at day d. Likewise, $C_{d,A}$ indicates the percentage of cloudiness for Aqua images after the introduction of fictitious clouds. The gap-filling procedure reclassifies $\Delta N_{c,T}$ either to snow or land. The comparison against the original Terra products determines three possible situations: overestimation errors (land to snow $L \rightarrow S$), underestimation errors ($S \rightarrow L$) and agreements (snow to snow $S \rightarrow S$ or land to land $L \rightarrow L$). Let a and b be the numbers of overestimations and underestimations, c and d the numbers of pixel correctly reclassified as snow or land. The overall degree of agreement D_A is (Paudel and Andersen, 2011):

$$D_A = 100 \cdot \frac{(c + d)}{\Delta N_{c,T}}. \quad (8)$$

HESSD
11, 3967–4015, 2014

The degree of disagreement is:

$$D_{\mathrm{D}} = 100 \cdot \frac{(a+b)}{\Delta N_{\mathrm{c,T}}}. \tag{9}$$

The latter is due to overestimations

$$O_{\mathrm{D}} = 100 \cdot \frac{a}{\Delta N_{\mathrm{c,T}}} \tag{10}$$

and underestimations

$$U_{\mathrm{D}} = 100 \cdot \frac{b}{\Delta N_{\mathrm{c,T}}}. \tag{11}$$

The overall accuracy is achieved by an average on the different performances, i, weighed on the percentage of pixels under examination per testing day.

$$\langle D_{\mathrm{A}} \rangle = \frac{\sum_i \left[D_{\mathrm{A},i} \cdot A_{(\mathrm{d,T})_i} \right]}{\sum_i A_{(\mathrm{d,T})_i}}. \tag{12}$$

The variance, σ^2, is calculated as

$$\sigma^2 = \frac{1}{\sum_i A_{(\mathrm{d,T})_i}} \sum_i A_{(\mathrm{d,T})_i} \cdot \left[D_{\mathrm{A},i} - \langle D_{\mathrm{A}} \rangle \right]^2. \tag{13}$$

The whole sample is composed by 25 days selected over the period 2003–2012. Results are shown in Table 6.

Overall, this improved approach shows a good level of accuracy in all seasons. For most of the tests the degree of agreement D_{A} reaches 96 %. A slight tendency to overestimate snow covers is evident; in spring, when melting rapidly reduces the snow-covered areas, the temporal filter in step 4 was expected to entail this effect. However,

HESSD
11, 3967–4015, 2014

overestimations occur also in autumn and winter. The maximum degree of disagreement (10 %) is obtained on 12 December 2012, after the application of a large cloud mask from 4 February 2012. Days before such date were characterized by a wide snowfall in the lowland, entailing a later fast evolution of ground conditions. Considering the area above 200 m a.s.l., we get $D_A = 95\,\%$ for the same testing day. A clear underestimation affects the accuracy of the procedure on 9 October 2011. Looking at the source maps this day appears as the first one with a well developed snow cover on the entire mountain region, shrinking back in next observations. The underestimation is mainly due to step 4, which finds lack of snow in the previous period. In general, autumn is characterized by snow areas under development and any type of filter looking backward may underestimate snow.

Tables 7 and 8 report the performances for each step of the procedure, relatively to 3 March 2012 and 10 December 2004. The same analysis was carried out for the whole sample. Overall, step 1 shows an high level of accuracy when outputs maps are compared to the original Terra products. We highly limited its intervention by masking the source maps of both satellites: such measure was necessary to involve even the other steps in the test. In general, more than 97 % of the cells classified by step 1 were correctly assigned to snow or land. Misclassifications may come either from changed ground conditions on the Aqua crossing times or from Aqua snow-mapping algorithm which uses MODIS band 7 instead of band 6 (Riggs et al., 2006). An example of poor performance for step 1 is shown in Table 8b for 10 December 2004. It was a cloudless day when snow cover had a wide distribution on the Alps. Terra provided a clear map with snow only on mountain reliefs. Aqua crossed the region about two hours later and its binary product shows snow in the western plain. Step 1 uses the latter to reclassify some additional clouds, contrasting with the source Terra product.

As already pointed out in Gafurov and Bárdossy (2009), step 2 has an high degree of accuracy. Even if it involves informations from close days, the efficiency is ensured by the requirement of stationary ground conditions within the temporal window. In our

HESSD
11, 3967–4015, 2014

analysis we never got a degree of agreement lower than 97 % on cloud pixels processed by step 2.

The regional snow and land lines defined in step 3 have shown an high efficiency whenever this method is involved in classifying a significant number of pixels. These elevations seem representative of the threshold altitudes above (below) which all cloud pixels are likely snow (land). On average the percentage of cloudiness processed by this step is lower than that of step 2. Nonetheless the degree of agreement provided for the majority of the days is comparable. On dates when its operation involves more than 3 % of the additional clouds (10 cases), its degree of accuracy never drops below 96 %. An example is 11 November 2009, where 21 % of the additional mask is cleaned by step 3, and the individual value of D_A reaches 99.2 %. On 8 December 2011 its contribution affects 12 % of the artificial clouds with an accuracy of 98.8 %. On 5 February 2004 it processes 14 % of the cover showing an individual D_A equal to 99.4 %. Moreover we verified that the daily average altitude of snow areas is generally lower than the elevation of the highest land pixel, thus allowing a wider action of the regional snow line approach.

Performances of steps 4 and 5 should be examined in days when previous steps leave out an high percentage of cloudiness. As matter of the fact, the last steps are called to close the procedure solving all cases of doubt: critical situations are those where ground conditions change quickly, or within the transition band where the snow line method does not intervene. Therefore a lower accuracy was foreseen and must be accepted. On days when it processes wide cloudy areas, the accuracy of the six days (backward) temporal filter is good. For example, on 31 March 2006 step 4 classifies by itself 89.5 % of the pixels artificially masked, providing a degree of agreement of 96.3 %. On 27 November 2004 its contribution involves 72.0 % of the additional cloudiness and classifies correctly the 95.1 % of them. A similar performance is provided on 17 May 2012 when its degree of agreement is about 97 % while removing 71 % of $\Delta N_{c,T}$.

HESSD
11, 3967–4015, 2014

A relatively extensive operation by step 5 takes place on 10 December 2004 when it processes about 10 % of the additional mask. Here, the degree of agreement reaches 95 %. Step 5 is involved even on 21 April 2004 and on 27 September 2006, processing about 5 % of $\Delta N_{c,T}$ with agreements of 93.5 and 99.8 %.

This step has been validated even individually on a reduced sample composed of six days from 2004 and four days from 2009. In the setup for the individual assessment, it intervenes after step 1 removing the whole cloud mask. It provided an average degree of accuracy of 95.0 %, with a tendency to underrate snow cover in spring and to overestimate in autumn. A second setup of step 5 was tested individually. Here, the first land observation after February and the first autumnal snow cover split the year in land and snow periods per pixel. This methodology, introduced by Gafurov and Bárdossy (2009), provides an overall degree of accuracy of 90.3 %. We are driven to think that improvements we suggested for individuating such macro-seasons perform properly. In particular, basing the start flag for snow season on more snow observations, we protected the performance from wide overestimates.

4.2.3 Comparison with other cloud removal procedures

We assessed the improvements produced by this procedure in comparison with other existing procedure for cloud reduction. First of all, we intend to realize whether the stepped procedure ensures any advantage compared to a mere backward temporal filter. We run the 7 days filter on the same sample, applied to the merged Aqua and Terra images (outputs by step 1). This filter was tested even in Parajka and Blöschl (2008) for Austria. Two results have to be provided. The first one is related to the percentages of cloud mask processed by each approach: while the new procedure, as in Gafurov and Bárdossy (2009), treats the entire mask, a filter limited to a preset time interval may leave out some cloudiness. The filter processes a fraction of $\Delta N_{c,T}$, equal to $A_{d,7d}/A_{d,T}$, where $A_{d,7d} \leq A_{d,T}$. Its degree of agreement is then evaluated on such percentage, $A_{d,7d}$. A second check concerns the reliability. Approximately, differences in the degrees of agreement should reflect the improvements due to steps 3 and 5,

HESSD
11, 3967–4015, 2014

since even our procedure introduces temporal filters in steps 2 and 4. The comparison reveals that the stepped procedure generates a concrete improvement when efficiency and accuracy are assessed in parallel. Completing the classification, it processes even those pixels hidden by clouds for more than 7 days that are certainly the hardest. And yet, it does not entail a decrease in the accuracy. An actually higher performance of the 7 days filter emerges only on 23 May 2009, when its degree of accuracy $D_{a,7d}$ outweighs the other of 0.5 %. Conversely, on three validation days the accuracy of the stepped procedure exceeds the temporal filter of more than 1.5 %. The percentages of additional clouds left out by the temporal filter are between 4 and 6 % for 5 days: focusing on our methodology, steps 2 and 4 require information on the previous days, as well as the 7 days filter. In such cases emerges the contributions of steps 3 and 5, allowing the classification of more pixels without entailing higher disagreement. Overall, the value of $\langle D_A \rangle$ of the proposed procedure is 95.7 %. On the other side, the individual temporal filter provides an average degree of agreement of 95.2 %. Moreover the variability in the accuracy of the performances is slightly lower in our procedure.

We also compared the procedure respect to the one proposed by Gafurov and Bárdossy (2009). Steps 1 and 2 are equal in these two stepped solutions. In Gafurov and Bárdossy (2009) the snow line and land line of step 3 are evaluated according to the highest land pixel and the lowest snow pixel, if the study area is at least 70 % cloud free. The temporal filter is not involved, while two spatial filters compose steps 4 and 5, comparing each cloud cell with ground conditions of the nearest cloud-free pixels (for a complete description see Gafurov and Bárdossy, 2009). The procedure is then completed with a "macro-cycle" approach working individually for each spatial unit, similar to our step 5. Differences lie in the way snow and land periods are evaluated. In Gafurov and Bárdossy (2009), the winter season coincides with the time window following the first snow observation, while land periods starts at the first land observation in spring. On the contrary, our step 5 checks ground conditions on more days before identifying the snow-land cycles.

HESSD
11, 3967–4015, 2014

Using the methodology by Gafurov and Bárdossy (2009), we got an overall $\langle D_A \rangle$ of 91.8 % followed by $\sigma = 7.2$ %. In most cases the two solutions show similar results; however, the combination of steps 4 and 5 in our procedure ensures much higher performances in closing the removal. The identification of the "snow period" through the first observation in autumn or winter, produces excessive overestimates for this case study. Micro-cycles are very common before winter, and the fluctuations of the area covered by snow can be very wide in a short time window. Moreover we found a very low effectiveness of spatial filters which work at the pixel scale, leading to slight contributions all over the seasons.

5 Conclusions

In this paper we investigated the use of MODIS products for snow mapping over Po river basin. The large-scale analysis, required when one deals with the major European rivers, often suggests the use of data from remote sensing. Snow cover maps for the whole domain require the adoption of a cloud removal procedure able to estimate ground condition beneath clouds, in order to preserve the daily resolution of the data.

The first question we would answer is: what is the obstruction from cloudiness on remote sensing snow products? Looking at our study region, this influence seems certainly more disturbing than what we expected. The average annual values of cloudiness are slightly lower than those found in Austria (Parajka and Blöschl, 2008). However, seasonal trends show that in the Alpine area this disturbance increases during the melting season. Focusing on spring, for most of the years (from 2003 to 2012) average values of cloud cover overcome the 70 % of the region which lies above 1000 m a.s.l. Spring is the most interesting period for hydrologic purposes since snow dynamics are faster and daily observations allow to follow gradually the patterns of melting, determining the contribution to streamflows. For this season, our analysis brings into question the real possibility of benefitting of maps with temporal resolution in the order of one day. Causes must be sought in the times of passage of the two satellites, that

HESSD
11, 3967–4015, 2014

lie between the late morning and the afternoon. Further investigation may be directed to a thorough identification of factors that determine seasonal and spatial patterns of cloudiness.

Several approaches have been proposed to reduce negative impacts of clouds on snow mapping: we tried to combine and improve steps from previous studies, in order to maximize the performance of the procedure in the considered case study. After some first attempts we noticed that methods already applied to other regions introduce assumptions that did not fit well for the climatic and topographic features of the Alps (Gafurov and Bárdossy, 2009; Gao et al., 2010; Paudel and Andersen, 2011). Northern Italy is mainly characterized by a range of elevations where snow undergoes several short cycles of accumulation and melt, thereby complicating any estimation of what lies under clouds. Our procedure requires only MODIS snow maps and a DEM of the domain, without additional data from other satellites nor information on land uses. It entails a computational effort slightly higher than a simple temporal filter, while completing the removing even when clouds hide the ground for extended time windows. Improvements are due to the introduction of the regional snow/land line step. When snow covers are well developed (mainly winter and spring), such method, similar to that of Parajka et al. (2010), plays a leading role both in terms of effectiveness and accuracy. Anyhow each step of the procedure has shown a good accuracy in the validation stage: the methodology ensured an average degree of accuracy of 95.7 % on the testing sample, showing a slight tendency to overestimate snow areas. Given our considerations on cloud obstruction on the reliefs, such a performance seems satisfactory.

We also want to highlight the good results provided by a simple temporal filter limited to 7 days, which uses the latest information available for each cell. However any restricted temporal filter leaves out a percentage of cloudiness which can be significant in the Alps, where clouds may cover the same area for several continuous days.

Approaches directed to the individuation of a typical condition for each cell on the basis of the period of the year (Gafurov and Bárdossy, 2009; Paudel and Andersen,

HESSD
11, 3967–4015, 2014

2011) seemed less suited to this environment. The identification of the first snow observation as the starting time of a window when a certain location is expected to be snow covered leads to excessive overestimates. We have got to verify that short-term snow covers are common over the transition altitudes, both in autumn and spring.

The removed-cloud maps provided by our procedure appear to be a reliable starting point from which it will be possible to derive information on snow resource for Po basin. The integration with snow depth measurements and snow density estimations will provide assessments on SWE amounts and fluctuations all over the last ten year. In long term, changes in such variables will reflect changing climatic forcings, thus impacting on economy and environment.

Supplementary material related to this article is available online at http://www.hydrol-earth-syst-sci-discuss.net/11/3967/2014/hessd-11-3967-2014-supplement.zip.

Acknowledgements. The research leading to these results has received funding from the Italian Ministry of Education, University and Research and the Italian Ministry of Environment, Land and Sea under GEMINA and NEXTDATA projects.

References

Ault, T. W., Czajkowski, K. P., Benko, T., Coss, J., Struble, J., Spongberg, A., Templin, M., and Gross, C.: Validation of the MODIS snow product and cloud mask using student and NWS cooperative station observations in the Lower Great Lakes Region, Remote Sens. Environ., 105, 341–353, 2006. 3970

Barnett, T. P., Adam, J. C., and Lettenmaier, D. P.: Potential impacts of a warming climate on water availability in snow-dominated regions, Nature, 438, 303–309, 2005. 3969

Bavera, D. and De Michele, C.: Snow water equivalent estimation in the Mallero basin using snow gauge data and MODIS images and fieldwork validation, Hydrological Processes, 23, 1961–1972, doi:10.1002/hyp.7328, 2009. 3970

HESSD
11, 3967–4015, 2014

Beniston, M.: Variations of snow depth and duration in the Swiss Alps over the last 50 years: links to changes in large-scale climatic forcings, Climatic Change, 36, 281–300, 1997. 3969, 3980

Beniston, M.: Climatic change in mountain regions: a review of possible impacts, in: Climate Variability and Change in High Elevation Regions: Past, Present & Future, vol. 15, edited by: Diaz, H. F., Springer Netherlands, 5–31, doi:10.1007/978-94-015-1252-7_2, 2003. 3969

Boé, J., Terray, L., Martin, E., and Habets, F.: Projected changes in components of the hydrological cycle in French river basins during the 21st century, Water Resour. Res., 45, W08426, doi:10.1029/2008WR007437, 2009. 3969

Dubayah, R. and Rich, P. M.: Topographic solar radiation models for GIS, Int. J. Geogr. Inf. Syst., 9, 405–419, doi:10.1080/02693799508902046, 1995. 3977

Etchevers, P., Golaz, C., Habets, F., and Noilhan, J.: Impact of a climate change on the Rhone river catchment hydrology, J. Geophys. Res., 107, ACL 6-1–ACL 6-18, doi:10.1029/2001JD000490, 2002. 3969

Gafurov, A. and Bárdossy, A.: Cloud removal methodology from MODIS snow cover product, Hydrol. Earth Syst. Sci., 13, 1361–1373, doi:10.5194/hess-13-1361-2009, 2009. 3970, 3973, 3974, 3975, 3976, 3977, 3979, 3984, 3986, 3989, 3991, 3992, 3993, 3994

Gao, Y., Xie, H., Lu, N., Yao, T., and Liang, T.: Toward advanced daily cloud-free snow cover and snow water equivalent products from Terra–Aqua MODIS and Aqua AMSR-E measurements, J. Hydrol., 385, 23–35, 2010. 3974, 3994

Haeberli, W. and Beniston, M.: Climate change and its impacts on glaciers and permafrost in the Alps, Ambio, 27, 258–265, 1998. 3969

Hagemann, S., Göttel, H., Jacob, D., Lorenz, P., and Roeckner, E.: Improved regional scale processes reflected in projected hydrological changes over large European catchments, Clim. Dynam., 32, 767–781, 2009. 3969

Hall, D. K. and Riggs, G. A.: Accuracy assessment of the MODIS snow products, Hydrol. Process., 21, 1534–1547, 2007. 3970, 3972, 3975, 3986

Hall, D. K., Riggs, G. A., and Salomonson, V. V.: Development of methods for mapping global snow cover using moderate resolution imaging spectroradiometer data, Remote Sens. Environ., 54, 127–140, 1995. 3972

Hall, D. K., Riggs, G. A., Salomonson, V. V., Barton, J., Casey, K., Chien, J., DiGirolamo, N., Klein, A., Powell, H., and Tait, A.: Algorithm theoretical basis document (ATBD) for the MODIS snow and sea ice-mapping algorithms, NASA GSFC, https://eospso.gsfc.nasa.gov/

HESSD
11, 3967–4015, 2014

sites/default/files/atbd/atbd_mod10.pdf (last access: April 2014), September 2001. 3972, 3985
Hock, R.: A distributed temperature-index ice-and snowmelt model including potential direct solar radiation, J. Glaciol., 45, 101–111, 1999. 3977
Hock, R.: Temperature index melt modelling in mountain areas, J. Hydrol. 282, 104–115, 2003. 3976
Hurkmans, R., Terink, W., Uijlenhoet, R., Torfs, P., Jacob, D., and Troch, P. A.: Changes in streamflow dynamics in the Rhine basin under three high-resolution regional climate scenarios, J. Climate, 23, 679–699, 2010. 3969
Junghans, N., Cullmann, J., and Huss, M.: Evaluating the effect of snow and ice melt in an Alpine headwater catchment and further downstream in the River Rhine, Hydrolog. Sci. J., 56, 981–993, 2011. 3969
Klein, A. G. and Barnett, A. C.: Validation of daily MODIS snow cover maps of the Upper Rio Grande River Basin for the 2000–2001 snow year, Remote Sens. Environ., 86, 162–176, 2003. 3970
Klein, A. G. and Stroeve, J.: Development and validation of a snow albedo algorithm for the MODIS instrument, Ann. Glaciol., 34, 45–52, 2002. 3972
Klein, A. G., Hall, D. K., and Riggs, G. A.: Improving snow cover mapping in forests through the use of a canopy reflectance model, Hydrol. Process., 12, 1723–1744, 1998. 3972
Kumar, L., Skidmore, A. K., and Knowles, E.: Modelling topographic variation in solar radiation in a GIS environment, Int. J. Geogr. Inf. Sci., 11, 475–497, doi:10.1080/136588197242266, 1997. 3977
Lenderink, G., Buishand, A., and van Deursen, W.: Estimates of future discharges of the river Rhine using two scenario methodologies: direct versus delta approach, Hydrol. Earth Syst. Sci., 11, 1145–1159, doi:10.5194/hess-11-1145-2007, 2007. 3969
Liang, T. G., Huang, X. D., Wu, C. X., Liu, X. Y., Li, W. L., Guo, Z. G., and Ren, J. Z.: An application of MODIS data to snow cover monitoring in a pastoral area: A case study in Northern Xinjiang, China, Remote Sens. Environ., 112, 1514–1526, 2008. 3970
Maurer, E. P., Rhoads, J. D., Dubayah, R. O., and Lettenmaier, D. P.: Evaluation of the snow-covered area data product from MODIS, Hydrol. Process., 17, 59–71, 2003. 3970
Molotch, N. P. and Margulis, S. A.: Estimating the distribution of snow water equivalent using remotely sensed snow cover data and a spatially distributed snowmelt model: A multi-resolution, multi-sensor comparison, Adv. Water Resour., 31, 1503–1514, 2008. 3970

HESSD
11, 3967–4015, 2014

Ohmura, A.: Physical basis for the temperature-based melt-index method, J. Appl. Meteorol., 40, 753–761, 2001. 3976

Parajka, J. and Blöschl, G.: Validation of MODIS snow cover images over Austria, Hydrol. Earth Syst. Sci., 10, 679–689, doi:10.5194/hess-10-679-2006, 2006. 3970, 3982

Parajka, J. and Blöschl, G.: Spatio-temporal combination of MODIS images – potential for snow cover mapping, Water Resour. Res., 44, W03406, doi:10.1029/2007WR006204, 2008. 3970, 3974, 3979, 3984, 3986, 3987, 3991, 3993

Parajka, J., Pepe, M., Rampini, A., Rossi, S., and Blöschl, G.: A regional snow-line method for estimating snow cover from MODIS during cloud cover, J. Hydrol., 381, 203–212, 2010. 3970, 3974, 3977, 3994

Paudel, K. P. and Andersen, P.: Monitoring snow cover variability in an agropastoral area in the Trans Himalayan region of Nepal using MODIS data with improved cloud removal methodology, Remote Sens. Environ., 115, 1234–1246, 2011. 3970, 3974, 3977, 3984, 3986, 3987, 3994

Riggs, G., Hall, D., and Salomonson, V.: MODIS snow products user guide to collection 5, Digital Media, http://nsidc.org/data/docs/daac/modis_v5/dorothy_snow_doc.pdf, last access: April 2014, p. 80, 2006. 3971, 3972, 3989

Salomonson, V. and Appel, I.: Estimating fractional snow cover from MODIS using the normalized difference snow index, Remote Sens. Environ., 89, 351–360, 2004. 3972

Salomonson, V. V. and Appel, I.: Development of the Aqua MODIS NDSI fractional snow cover algorithm and validation results, IEEE T. Geosci. Remote, 44, 1747–1756, 2006. 3972

Schaefli, B., Hingray, B., Niggli, M., and Musy, A.: A conceptual glacio-hydrological model for high mountainous catchments, Hydrol. Earth Syst. Sci., 9, 95–109, doi:10.5194/hess-9-95-2005, 2005. 3976

Shabalova, M., van Deursen, W., and Buishand, T.: Assessing future discharge of the river Rhine using regional climate model integrations and a hydrological model, Clim. Res., 23, 233–246, 2003. 3969

Simic, A., Fernandes, R., Brown, R., Romanov, P., and Park, W.: Validation of VEGETATION, MODIS, and GOES + SSM/I snow-cover products over Canada based on surface snow depth observations, Hydrol. Process., 18, 1089–1104, doi:10.1002/hyp.5509, 2004. 3970

Tekeli, A. E., Akyürek, Z., Arda Şorman, A., Şensoy, A., and Ünal Şorman, A.: Using MODIS snow cover maps in modeling snowmelt runoff process in the eastern part of Turkey, Remote Sens. Environ., 97, 216–230, 2005. 3970

HESSD

11, 3967–4015, 2014

Valt, M. and Cianfarra, P.: Recent snow cover variability in the Italian Alps, Cold Reg. Sci. Technol., 64, 146–157, 2010. 3980

Vanham, D.: The Alps under climate change: implications for water management in Europe, J. Water Clim. Change, 3, 197–206, 2012. 3969

Zhou, X., Xie, H., and Hendrickx, J. M.: Statistical evaluation of remotely sensed snow-cover products with constraints from streamflow and SNOTEL measurements, Remote Sens. Environ., 94, 214–231, 2005. 3970

HESSD

11, 3967–4015, 2014

Table 1. C_a ($Z > z_T$): mean annual cloud cover fraction for different altitude thresholds over Po river basin.

	z_T = 0 m a.s.l.		z_T = 1000 m a.s.l.		z_T = 2000 m a.s.l.	
Year	Aqua	Terra	Aqua	Terra	Aqua	Terra
2003	0.47	0.46	0.57	0.51	0.58	0.52
2004	0.57	0.54	0.66	0.60	0.66	0.59
2005	0.52	0.50	0.61	0.52	0.63	0.54
2006	0.52	0.49	0.60	0.54	0.61	0.54
2007	0.48	0.46	0.58	0.53	0.62	0.54
2008	0.56	0.53	0.66	0.59	0.66	0.58
2009	0.54	0.50	0.62	0.55	0.63	0.56
2010	0.59	0.56	0.67	0.60	0.67	0.60
2011	0.46	0.44	0.57	0.51	0.59	0.52
2012	0.52	0.49	0.63	0.56	0.65	0.57

HESSD
11, 3967–4015, 2014

Table 2. Mean cloud cover fraction over Po river basin averaged per quarter from MOD10A1.

Year	J F M	A M J	J A S	O N D
2003	0.44	0.46	0.31	0.62
2004	0.63	0.52	0.39	0.63
2005	0.48	0.47	0.45	0.59
2006	0.54	0.56	0.38	0.49
2007	0.58	0.48	0.32	0.47
2008	0.52	0.60	0.38	0.62
2009	0.55	0.52	0.34	0.62
2010	0.68	0.55	0.36	0.64
2011	0.56	0.43	0.31	0.47
2012	0.44	0.56	0.36	0.60

HESSD
11, 3967–4015, 2014

Table 3. Mean cloud cover fraction over Po river basin averaged per quarter from MOD10A1, $Z > 1500$ m a.s.l.

Year	J F M	A M J	J A S	O N D
2003	0.47	0.64	0.41	0.59
2004	0.60	0.68	0.52	0.61
2005	0.50	0.61	0.55	0.51
2006	0.54	0.68	0.52	0.45
2007	0.61	0.66	0.44	0.46
2008	0.51	0.77	0.50	0.60
2009	0.54	0.67	0.46	0.57
2010	0.64	0.72	0.47	0.62
2011	0.54	0.64	0.45	0.46
2012	0.50	0.71	0.48	0.59

HESSD
11, 3967–4015, 2014

Table 4. Mean annual cloud cover fraction remaining after each step for Po river basin.

Year	Aqua	Terra	Step 1	Step 2	Step 3	Step 4
2003	0.470	0.460	0.374	0.207	0.174	0.016
2004	0.570	0.540	0.455	0.308	0.282	0.039
2005	0.520	0.500	0.417	0.270	0.225	0.015
2006	0.520	0.490	0.403	0.244	0.207	0.021
2007	0.480	0.460	0.374	0.231	0.192	0.018
2008	0.560	0.530	0.452	0.308	0.273	0.047
2009	0.540	0.500	0.425	0.283	0.243	0.024
2010	0.590	0.560	0.478	0.332	0.282	0.038
2011	0.460	0.440	0.363	0.233	0.197	0.025
2012	0.520	0.490	0.407	0.258	0.213	0.018

HESSD
11, 3967–4015, 2014

Table 5. Average monthly cloud cover fraction remaining after each step for year 2010.

Month	Aqua	Terra	Step 1	Step 2	Step 3	Step 4
Jan	0.755	0.703	0.582	0.430	0.311	0.057
Feb	0.751	0.691	0.622	0.451	0.370	0.024
Mar	0.675	0.643	0.582	0.447	0.404	0.052
Apr	0.555	0.504	0.441	0.228	0.183	0.013
May	0.654	0.662	0.569	0.450	0.427	0.149
Jun	0.517	0.482	0.393	0.251	0.220	0.051
Jul	0.286	0.232	0.151	0.033	0.031	0.002
Aug	0.420	0.390	0.306	0.108	0.088	0.009
Sep	0.502	0.445	0.370	0.176	0.129	0.003
Oct	0.619	0.586	0.516	0.388	0.329	0.004
Nov	0.734	0.702	0.641	0.533	0.461	0.027
Dec	0.656	0.642	0.576	0.500	0.442	0.063

HESSD
11, 3967–4015, 2014

Table 6. Overall accuracy of the cloud removal methodology tested on several days and comparison with a basic 7 days temporal filter. Values in [%].

Clear-sky days	Cloudy days	$A_{d,A}$	$A_{d,T}$	D_A	O_D	U_D	$A_{d,7d}/A_{d,T}$	$D_{A,7d}$
5 Feb 2004	2 Feb 2004	75.1	95.9	93.2	5.5	1.3	99.4	92.1
19 Mar 2004	24 Mar 2004	78.9	71.5	95.7	2.2	2.1	100.0	95.6
21 Apr 2004	29 Apr 2004	77.1	85.7	96.1	3.6	0.3	95.5	96.1
19 May 2004	22 May 2004	78.7	88.6	97.7	1.2	1.1	100.0	97.3
27 Nov 2004	20 Jul 2004	66.5	59.5	94.1	4.9	1.0	100.0	94.4
10 Dec 2004	16 Dec 2004	74.4	75.5	95.6	3.8	0.6	95.5	93.9
26 Apr 2005	21 Oct 2005	90.2	93.0	96.7	2.6	0.7	96.6	97.0
20 Dec 2005	14 May 2005	52.0	78.2	95.2	3.1	1.7	100.0	94.4
13 Feb 2006	27 Mar 2006	78.8	85.9	92.9	4.1	3.0	100.0	92.4
31 Mar 2006	19 Oct 2006	85.2	84.8	96.6	2.4	1.0	99.6	96.6
15 Jun 2006	3 Oct 2006	82.4	83.3	99.6	0.1	0.3	100.0	99.5
27 Sep 2006	21 Nov 2006	87.5	88.1	97.3	2.2	0.5	99.2	97.2
1 Dec 2006	1 Apr 2006	87.5	88.1	96.5	2.8	0.7	96.3	96.3
1 May 2009	10 Mar 2009	80.0	79.3	97.3	2.1	0.6	95.2	96.3
15 Feb 2009	3 Feb 2009	84.2	90.8	95.7	2.6	1.7	99.8	95.6
23 May 2009	13 Nov 2009	86.8	85.9	96.2	3.6	0.2	98.7	96.7
11 Nov 2009	29 Nov 2009	94.2	96.0	93.3	4.6	2.1	93.9	91.7
9 Feb 2011	20 Apr 2011	80.7	84.1	95.9	3.0	1.1	100.0	94.7
2 Apr 2011	9 Dec 2011	90.2	95.5	96.8	3.0	0.2	98.6	97.1
8 Dec 2011	14 Oct 2011	38.3	57.7	96.4	2.5	1.1	99.9	96.1
9 Oct 2011	15 Dec 2011	69.3	95.7	93.5	1.8	4.7	100.0	92.9
3 Mar 2012	22 Jan 2012	63.7	84.1	97.3	2.1	0.6	100.0	97.3
17 May 2012	18 Nov 2012	88.5	96.0	96.8	1.6	1.6	99.9	96.7
7 Nov 2012	22 Dec 2012	93.4	92.0	96.5	2.7	0.8	99.7	95.0
12 Dec 2012	4 Feb 2012	85.2	91.2	90.0	8.3	1.7	99.7	90.1
Weighted average				95.7	3.1	1.2	98.6	95.2
σ				2.0				2.3

HESSD
11, 3967–4015, 2014

Table 7. Cloud, land and snow percentages (C_d, L_d, S_d) in two clear-sky maps on 3 March 2012 and 10 December 2004, and percentages after the application of the additional cloudiness (A_d).

(a) 3 March 2012				
3 Mar 2012	C_d	L_d	S_d	A_d
Source Aqua SCA	13.9 %	77.7 %	8.4 %	[–]
Source Terra SCA	7.5 %	82.9 %	9.6 %	[–]
Masked Aqua SCA	77.6 %	21.9 %	0.5 %	63.7 %
Masked Terra SCA	91.6 %	7.9 %	0.5 %	84.0 %
(b) 10 December 2004				
10 Dec 2004	C_d	L_d	S_d	A_d
Source Aqua SCA	9.6 %	67.2 %	23.2 %	[–]
Source Terra SCA	6.9 %	76.9 %	16.2 %	[–]
Masked Aqua SCA	84.0 %	11.3 %	4.7 %	74.4 %
Masked Terra SCA	82.4 %	12.9 %	4.7 %	75.5 %

HESSD
11, 3967–4015, 2014

Table 8. Results of the validation step by step on 3 March 2012 and 10 December 2004.

(a) 3 March 2012

3 Mar 2012		Disagreement		Agreement		Individual accuracy	
	Contribution	$S \rightarrow L$	$L \rightarrow S$	$S \rightarrow S$	$L \rightarrow L$	Individual D_D	Individual D_A
Step 1	23.1 %	0.0 %	0.3 %	0.2 %	22.6 %	1.3 %	98.7 %
Step 2	27.0 %	0.1 %	0.2 %	2.5 %	24.2 %	1.0 %	99.0 %
Step 3	6.4 %	0.0 %	0.1 %	0.9 %	5.4 %	1.1 %	98.9 %
Step 4	43.5 %	0.5 %	1.5 %	6.5 %	35.0 %	4.5 %	96.5 %
Step 5	0.0 %	0.0 %	0.0 %	0.0 %	0.0 %	0.0 %	0.0 %
Overall	100.0 %	0.6 %	2.1 %	10.1 %	87.2 %	2.7 %	97.3 %

(b) 10 December 2004

10 Dec 2004		Disagreement		Agreement		Individual accuracy	
	Contribution	$S \rightarrow L$	$L \rightarrow S$	$S \rightarrow S$	$L \rightarrow L$	Individual D_D	Individual D_A
Step 1	7.0 %	0.0 %	0.8 %	1.4 %	4.8 %	11.6 %	88.4 %
Step 2	72.4 %	0.4 %	1.0 %	10.8 %	60.3 %	2.0 %	98.0 %
Step 3	6.2 %	0.0 %	0.1 %	1.0 %	5.1 %	2.1 %	97.9 %
Step 4	4.6 %	0.1 %	1.5 %	1.2 %	1.7 %	34.8 %	65.2 %
Step 5	9.8 %	0.1 %	0.4 %	0.2 %	9.1 %	5.1 %	94.9 %
Overall	100.0 %	0.6 %	3.8 %	14.6 %	81.0 %	4.5 %	95.5 %

HESSD
11, 3967–4015, 2014

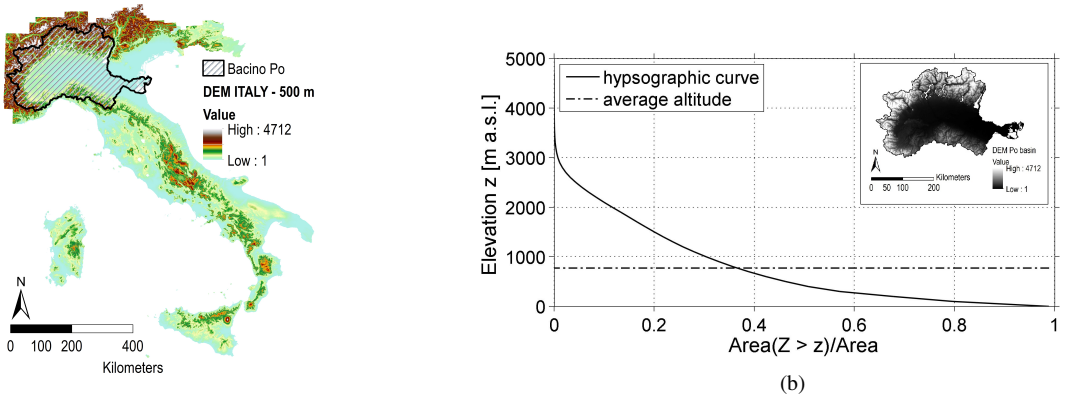

(a) (b)

Fig. 1. (a) DEM of Italy at 500 m spatial resolution with the contour line of Po basin. **(b)** Hypsographic curve of Po river basin derived from the DEM.

HESSD
11, 3967–4015, 2014

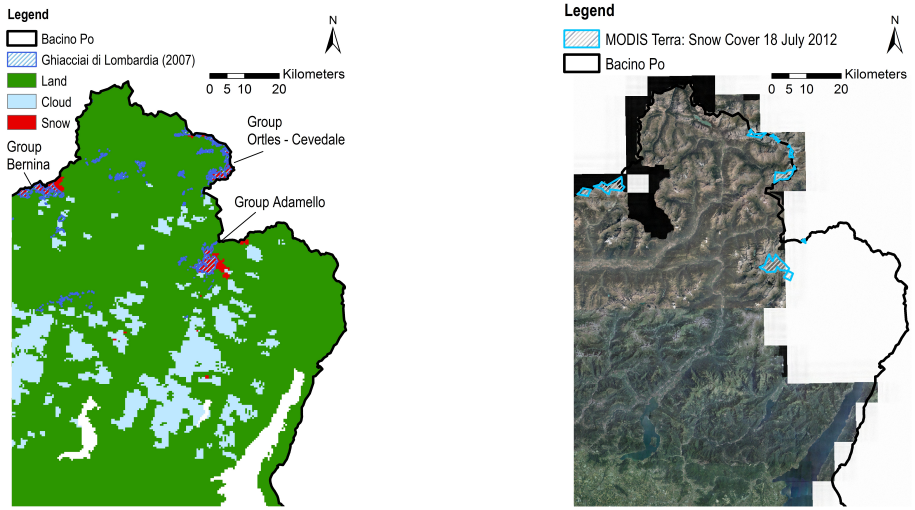

(a) 2005

(b) 2012

Fig. 2. (a) Comparison between the digital map of Lombardy's glaciers (sketched in blue) and the snow distribution (red) from MYD10A1 at the end of June 2005 (source Regione Lombardia https://www.dati.lombardia.it/Territorio/Ghiacciai-e-Nevai). **(b)** Snow polygon derived from MOD10A1 of 18 July 2012 overlapped on the orthophoto AGEA 2012 of Lombardia. The latter is a composite image from air flights operated at the beginning of September 2012 (source Regione Lombardia http://www.cartografia.regione.lombardia.it).

HESSD
11, 3967–4015, 2014

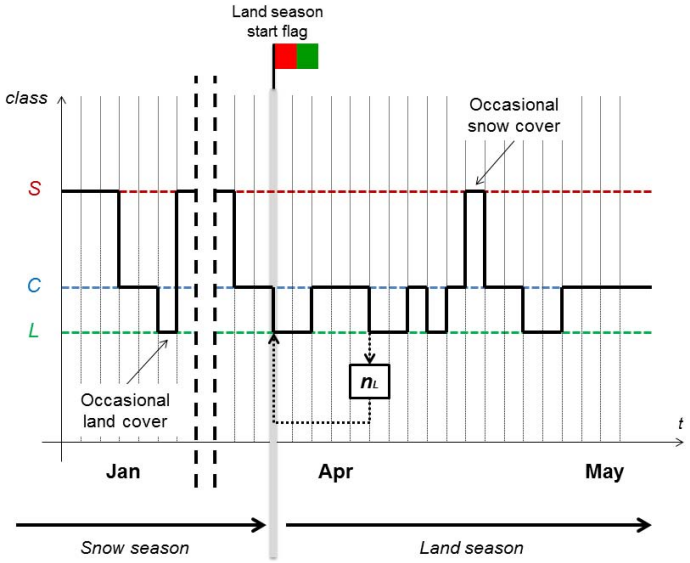

Fig. 3. Criterion for identifying the start of the land season. The same rule is applied to the snow-start flag, in autumn or winter. More land/snow observations are needed in spring/autumn to split the year into two periods. The black line represents the series of observations for a reference pixel across the melting season.

HESSD
11, 3967–4015, 2014

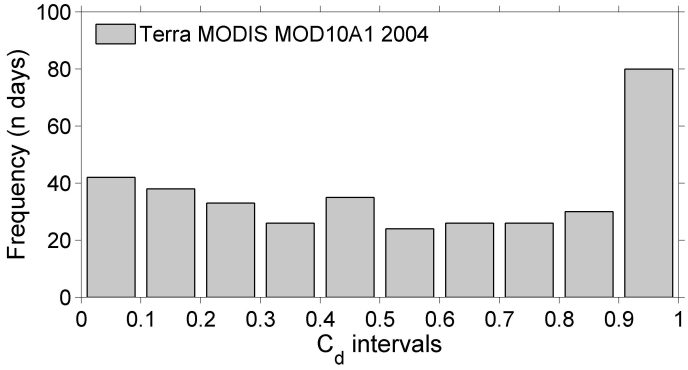

Fig. 4. Absolute frequency of the daily cloud percentage C_d from Terra MOD10A1: year 2004.

HESSD
11, 3967–4015, 2014

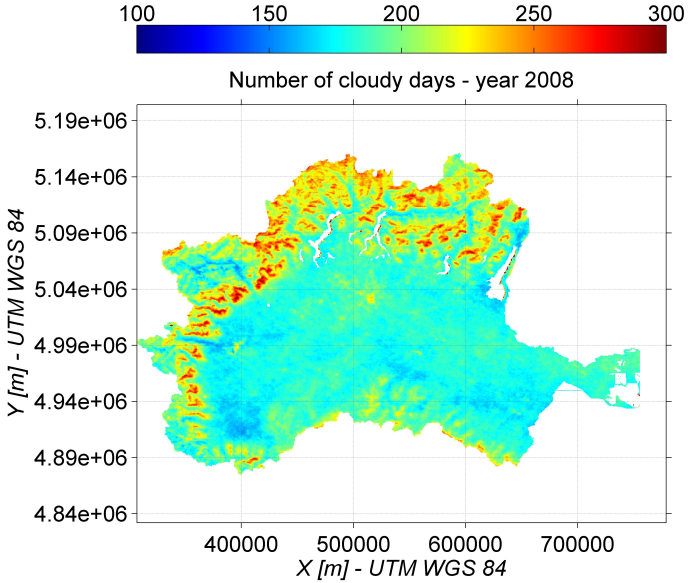

Fig. 5. Number of cloud observations per pixel from MOD10A1 SCA product (0 - 365 days): year 2008.

HESSD
11, 3967–4015, 2014

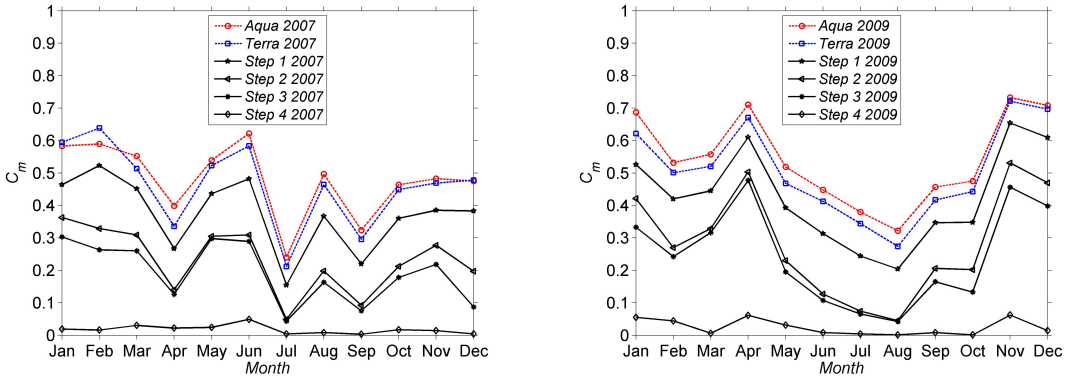

(a) 2007 (b) 2009

Fig. 6. C_m, average monthly values of C_d remaining after the implementation of each step for year 2007 **(a)** and 2009 **(b)**.

HESSD
11, 3967–4015, 2014

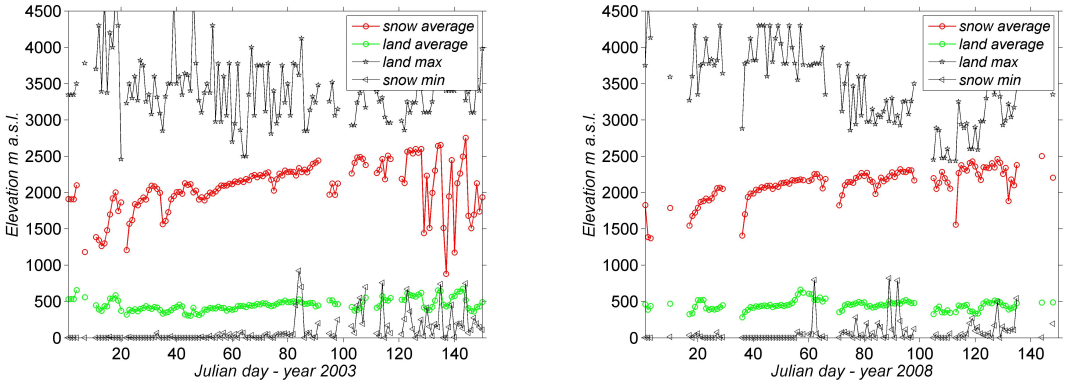

(a) 2003 (b) 2008

Fig. 7. Regional snow and land lines from January to May in comparison with the elevations of the highest land pixel and the lowest snow pixel, year 2003 **(a)** and 2008 **(b)**. Values are provided only when output maps by step 2 are less than 50 % cloud covered.

HESSD
11, 3967–4015, 2014

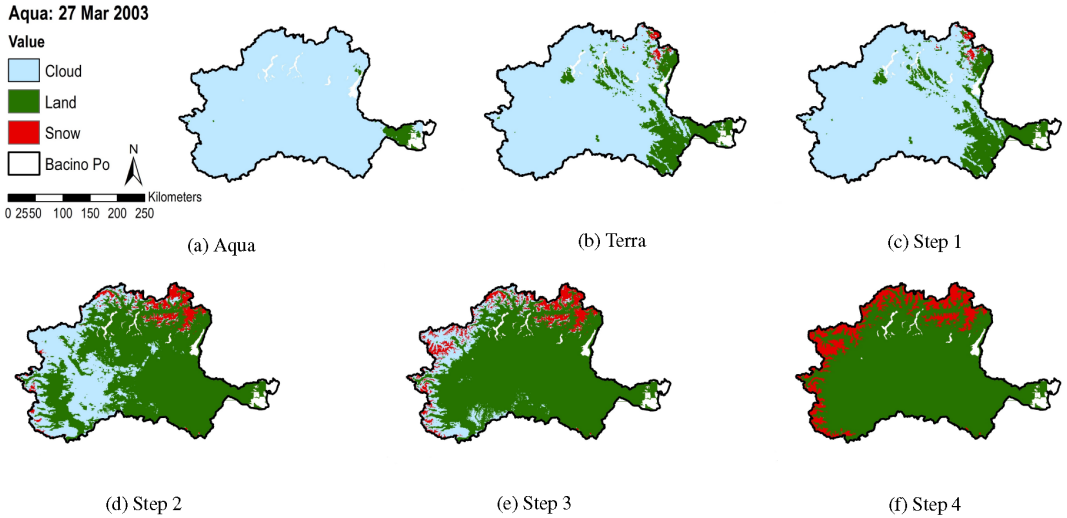

Fig. 8. Cloud removal procedure applied to 27 March 2003. Aqua and Terra maps have a cloud coverage of 98 and 83 %, respectively. Step 2 leaves out a cloud coverage of 29 %. The intervention of step 3 affects 14 % of the domain and step 4 closes the cleaning procedure.

HESSD
11, 3967–4015, 2014